Surname *et al. Energy Mater* Year;Volume:Number
DOI: 10.20517/energymater.2021.xx

Energy Materials

Supplementary Material

Highly crystalline covalent triazine frameworks modified separator for lithium metal batteries

Yun Wang, Ruixue Sun, Yi Chen, Xuyang Wang, Yufei Yang, Xiaoyan Wang, Hui Nie*, Xingping Zhou, Bien Tan*, Xiaolin Xie

Key Laboratory of Material Chemistry for Energy Conversion and Storage, Ministry of Education, School of Chemistry and Chemical Engineering, Huazhong University of Science and Technology, Wuhan 430074, Hubei, China.

Correspondence to: Dr. Hui Nie, Key Laboratory of Material Chemistry for Energy Conversion and Storage, Ministry of Education, School of Chemistry and Chemical Engineering, Huazhong University of Science and Technology, 1037 Luoyu Road, Hongshan District, Wuhan 430074, Hubei China. E-mail: huinie@hust.edu.cn; Dr. Bien Tan, Key Laboratory of Material Chemistry for Energy Conversion and Storage, Ministry of Education, School of Chemistry and Chemical Engineering, Huazhong University of Science and Technology, 1037 Luoyu Road, Hongshan District, Wuhan 430074, Hubei, China. E-mail: bien.tan@mail.hust.edu.cn

EXPERIMENTAL

Materials

Benzene-1,4-dicarbonitrile, dimethyl sulfoxide (DMSO), cesium carbonate (Cs_2CO_3), tetrahydrofuran (THF), hydrochloric acid, acetone, ether and ethanol (EtOH) were analysis grade and purchased from National Medicines Corporation Ltd. of China. Lithium bis(trimethylsilyl)azanide (1.0mol/L in THF) ($LiN(SiMe_3)_2$) and terephthalaldehyde were obtained from Aldrich Chemical Co. and used as received. Other reagents of analytical grade were utilized without further purification.

Preparation of AM-CTF and HC-CTF

Both AM-CTF and HC-CTF were synthesized using an amidine-based polycondensation method, with terephthalamidine dihydrochloride and terephthalaldehyde as monomers and Cs_2CO_3 as the catalyst. The key difference lies in the monomer feeding process: AM-CTF synthesis involved adding the monomer all at once, while HC-CTF synthesis was achieved by controlling the addition rate of the monomer terephthalaldehyde. This control, in turn, regulates the nucleation process of the crystals, leading to the formation of HC-CTF.

Synthesis of terephthalamidine dihydrochloride:

Added 1.92 g of benzene-1,4-dicarbonitrile to 30 mL of THF, slowly introducing 60 mL of 1 M $LiN(SiMe_3)_2$ solution drop by drop under an argon atmosphere at 0 °C. Stirred the mixture for 3 hours at 25 °C to obtain a clarified caramel-colored solution. After cooling to 0 °C, slowly added 60 mL of 6 M HCl-EtOH solution dropwise, brought slowly to room temperature and stirred overnight. Filtered, washed with ether, recrystallized in H_2O-EtOH mixture and dried to obtain brown fine needle-like crystals of terephthalamidine dihydrochloride.

Synthesis of AM-CTF:

100.8 mg of terephthalaldehyde, 352.8 mg of terephthalamidine dihydrochloride, and 1075.2 mg of Cs_2CO_3 were dissolved in a mixture of 7.5 mL of DMSO. The mixture was stirred at 60 °C, 80 °C, 100 °C and 120 °C under air atmosphere for 12 hours. The concentration of the solution changed from dilute to thick, and the color transitioned from

light red to dark red. After the reaction, the solution was filtered, washed with dilute hydrochloric acid, deionized water, acetone and THF in turn, and then dried to obtain yellow AM-CTF powder.

Synthesis of HC-CTF:

Preparation of solution A: The solution of terephthalaldehyde (67 mg, 0.5 mmol) and DMSO (20 mL) was stirred at 50 ℃ for 30 minutes.

Preparation of solution B: Added terephthalamidine dihydrochloride (0.235 mg, 1.0 mmol) and Cs_2CO_3 (490 mg, 1.5 mmol) to DMSO solution (10 mL) and stirred at 100 ℃ for 30 minutes.

Controlled feed rate synthesis of HC-CTF: Solution A was added dropwise at 30 μL/min to solution B via a peristaltic pump at 100 °C. The process lasted for about 10 hours, totaling 24 hours. Subsequently, a condenser tube with a drying tube was attached to the flask, which was raised to 180 °C and maintained for 48 hours. The resulting yellow precipitate was washed with dilute hydrochloric acid to remove the residual Cs_2CO_3, further washed with water, ethanol and THF. The filtered solid was freeze-dried for 24 hours to obtain HC-CTF.

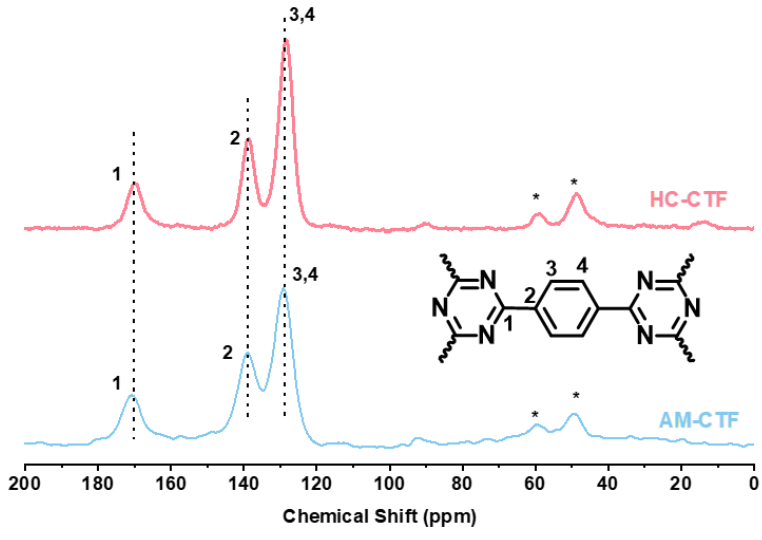

Supplementary Figure 1. CP-MAS ^{13}C NMR spectra of AM-CTF and HC-CTF.

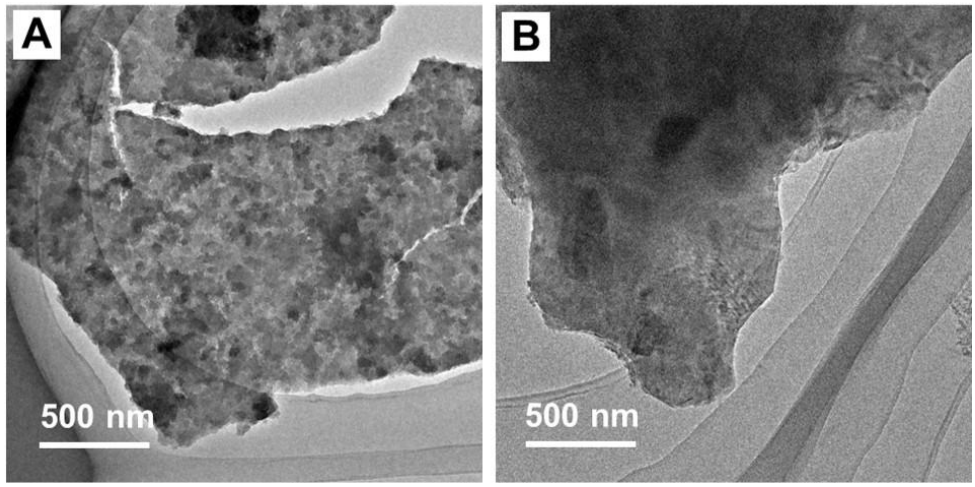

Supplementary Figure 2. TEM images of (A) AM-CTF and (B) HC-CTF.

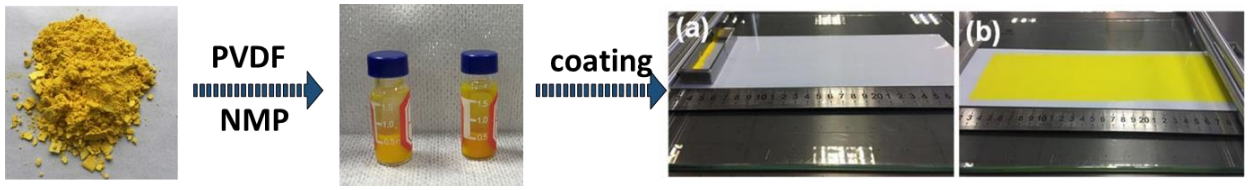

Supplementary Figure 3. Preparation process of CTF-coated separators.

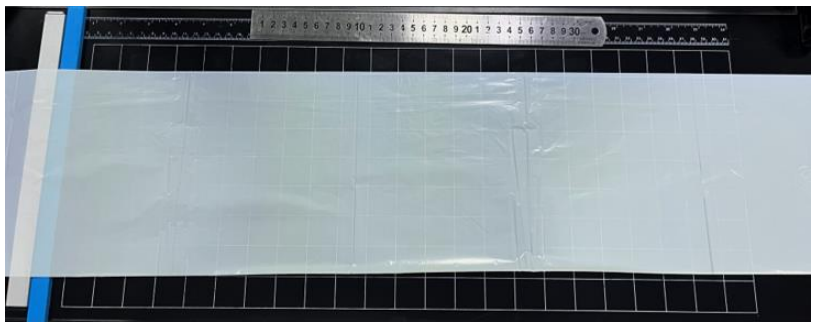

Supplementary Figure 4. The photo of large-size CTF modified PE separator.

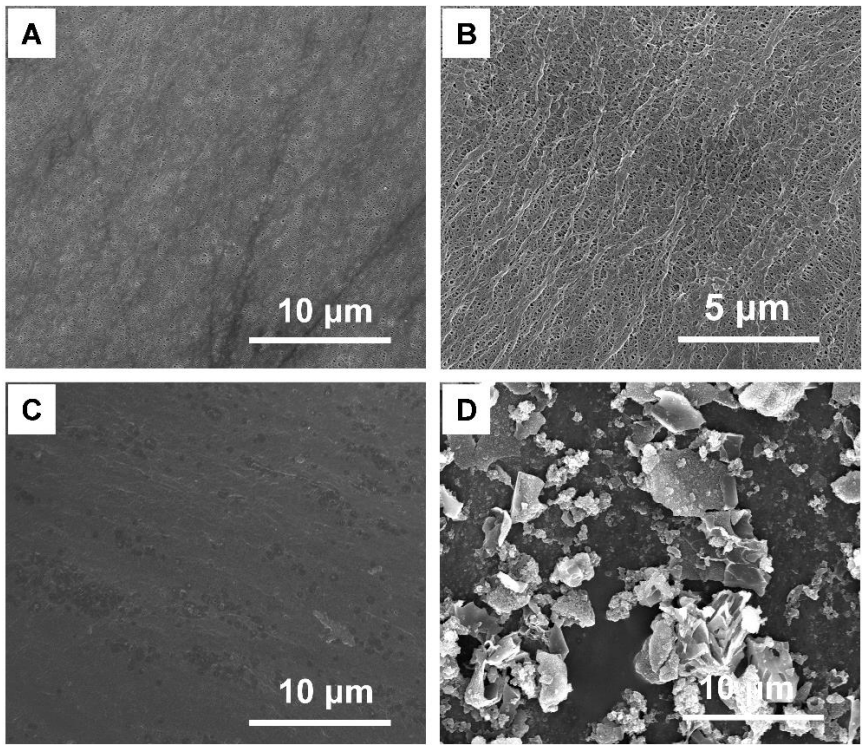

Supplementary Figure 5. (A, B) Top-view SEM images of PE separator; high-magnification Top-view SEM image of (C) AM-CTF-PE and (D) HC-CTF-PE separators.

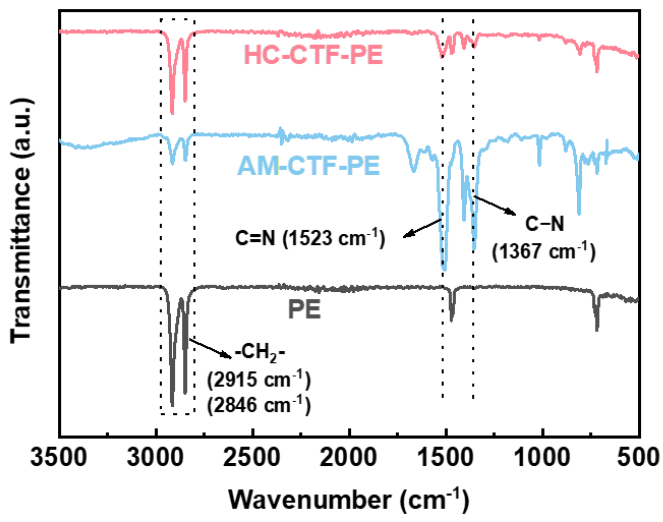

Supplementary Figure 6. FT−IR spectra of the PE, AM-CTF-PE, and HC-CTF-PE separators.

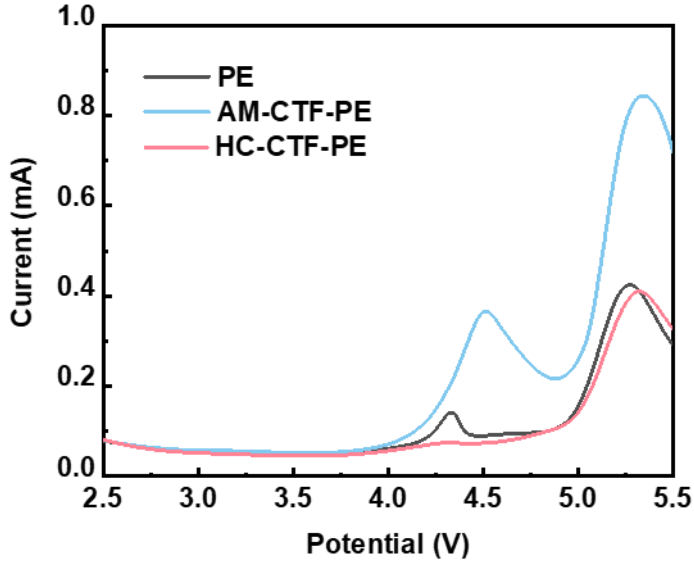

Supplementary Figure 7. LSV curves of the PE, AM-CTF-PE and HC-CTF-PE separators.

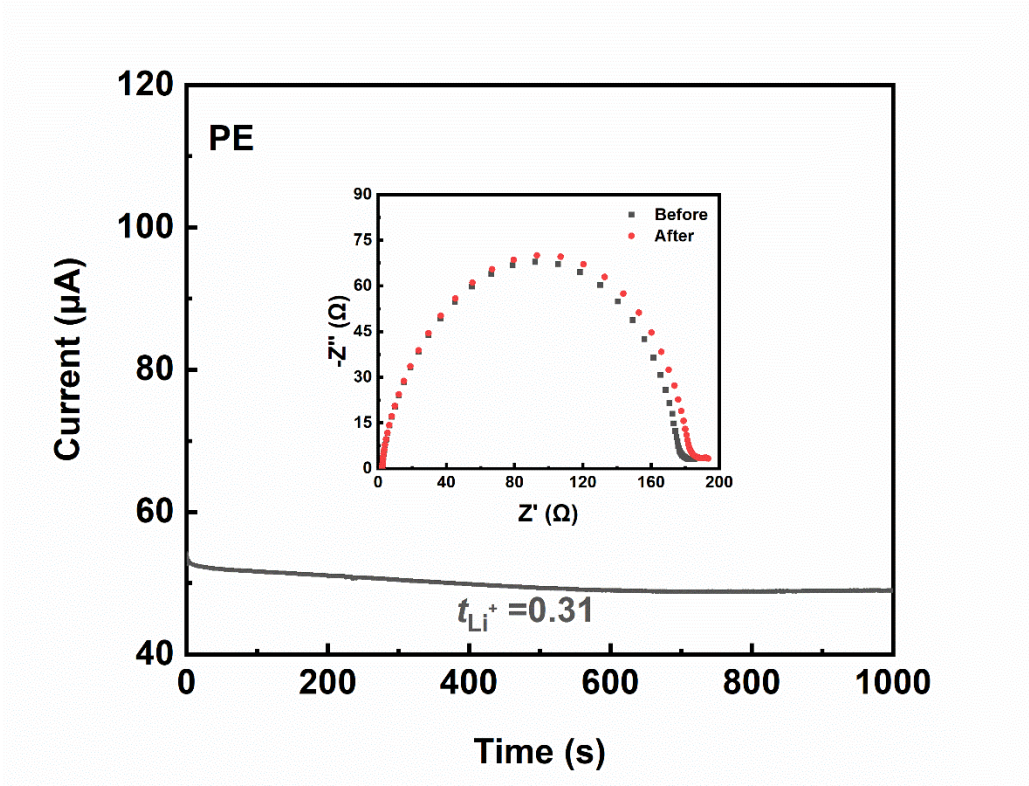

Supplementary Figure 8. Chronoamperometry profiles of PE separators. Inset are the AC impedance spectra before and after polarization.

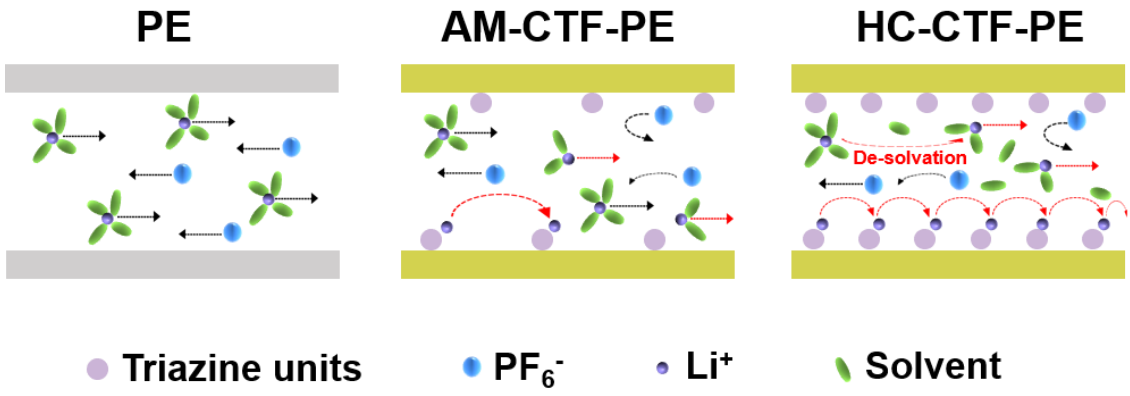

Supplementary Figure 9. Schematic illustrations of ion transport process in PE, AM-CTF-PE and HC-CTF-PE separators.

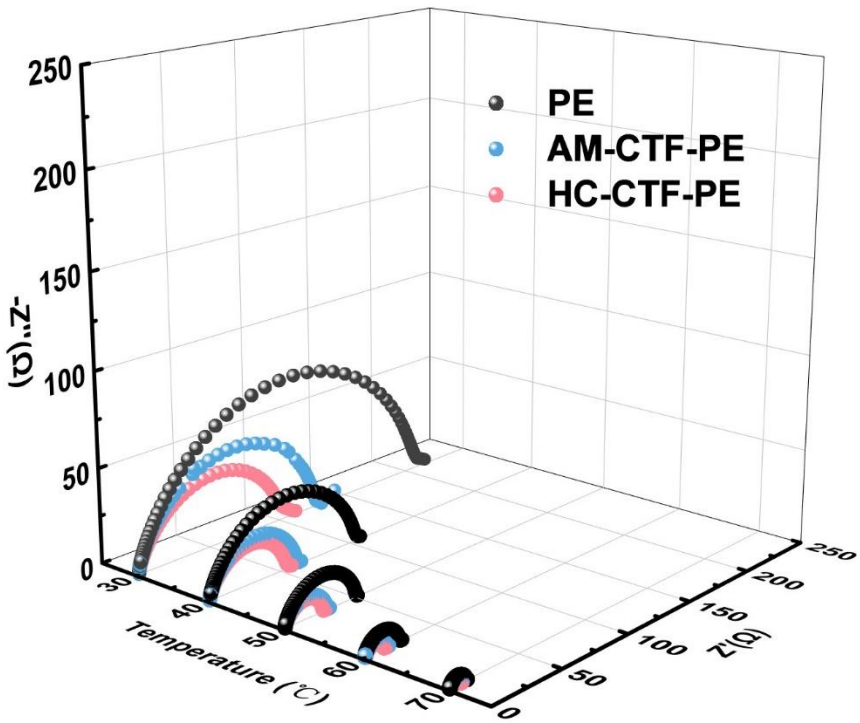

Supplementary Figure 10. Nyquist plots of the PE, AM-CTF-PE and HC-CTF-PE separators at different temperatures based on EIS measurements.

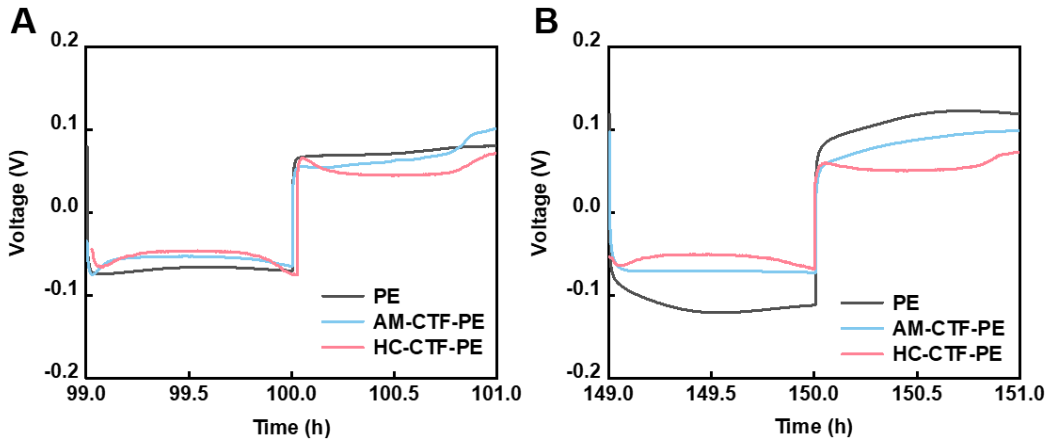

Supplementary Figure 11. Voltage–time profiles of Li//Li symmetric cells assembled with PE, AM-CTF-PE and HC-CTF-PE separators at different cycling time.

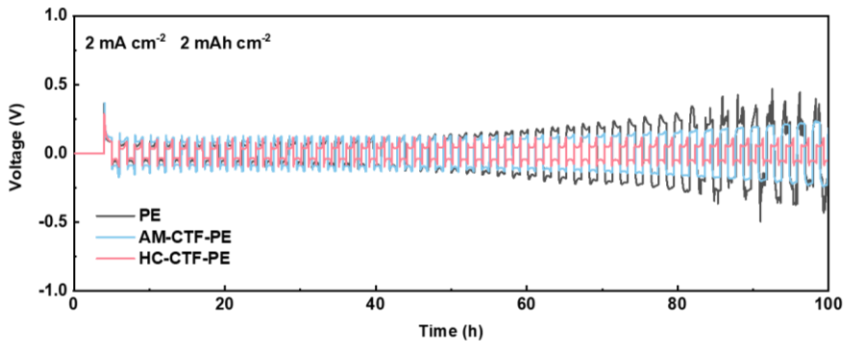

Supplementary Figure 12. Voltage-time profiles of Li//Li symmetric cells assembled with PE, AM-CTF-PE and HC-CTF-PE separators at 2 mA cm^{-2} with a capacity of 2 mAh cm^{-2}

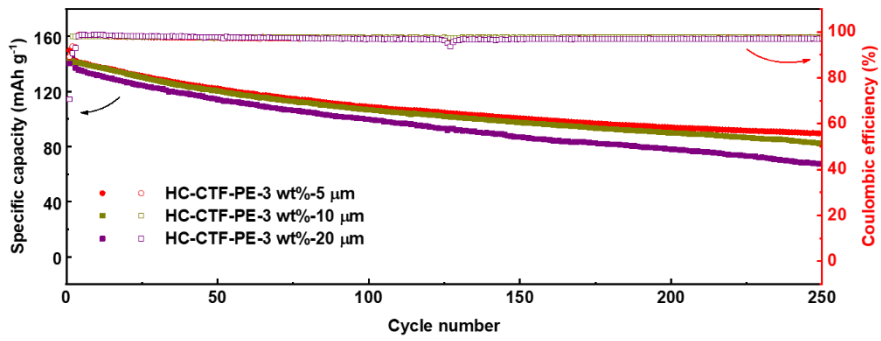

Supplementary Figure 13. Long-term cycling stability of LFP/Li cells at 1 C with HC-CTF-PE separators with different thickness. HC-CTF-PE-3 wt%-5 μm, HC-CTF-PE-3

wt%-10 μm and HC-CTF-PE-3 wt%-20 μm are prepared by adjusting the distance of blade to PE surface of 5, 10 and 20 μm, respectively, during the slurry spreading procedure.

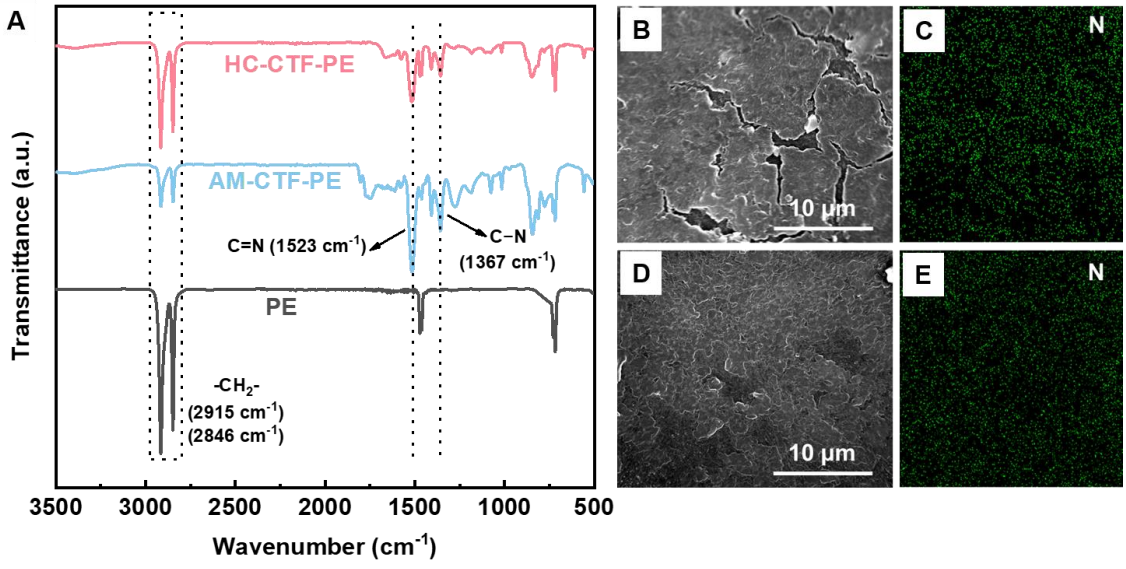

Supplementary Figure 14 (A) FT−IR spectra of PE, AM-CTF-PE and HC-CTF-PE separators after 100 cycles at 1 C of LFP/Li cells; (B) FE-SEM image and (C) EDS mapping of N elements of AM-CTF-PE separators after 100 cycles at 1 C of LFP/Li cells; (D) FE-SEM image and (E) EDS mapping of N elements of HC-CTF-PE separators after 100 cycles at 1 C of LFP/Li cells.

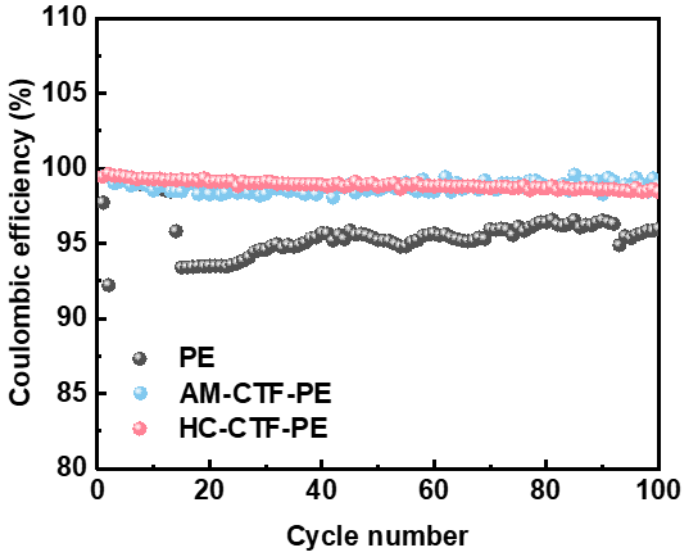

Supplementary Figure 15. The enlarged image of Coulombic efficiency for the cycling performance at 3 C with the $LiFePO_4$ loading of 1.58 mg cm^{-2}.

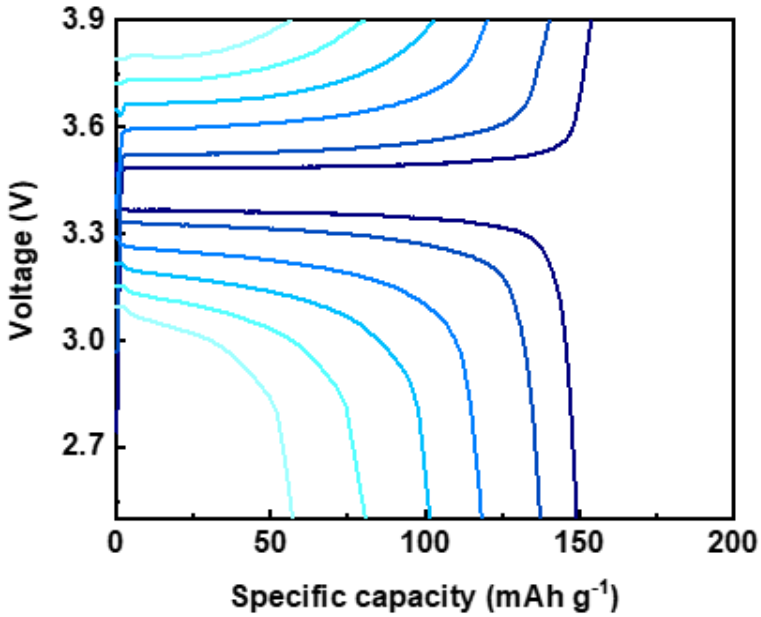

Supplementary Figure 16. Charge-discharge curves of AM-CTF-PE separator at various current densities of 0.5-5 C.

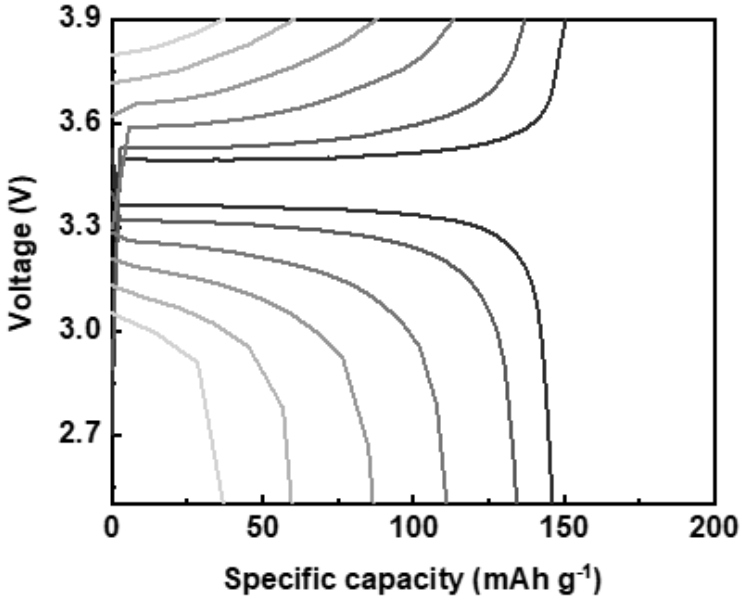

Supplementary Figure 17. Charge-discharge curves of PE separator at various current densities of 0.5-5 C.

Supplementary Table 1. The values of the BET surface area, pore volume and the porosity of the AM-CTF-PE and HC-CTF-PE separators.

	BET surface area (m^2/g)	**pore volume (cm^3/g)**	**Porosity (%)**
AM-CTF-PE	26.33	0.274	42.3%
HC-CTF-PE	34.34	0.308	46.8%

Supplementary Table 2. The values of the thickness of the separators, area of the stainless electrode, and bulk resistance for ionic conductivity calculations.

	Electrode area (cm^2)	**Thickness (μm)**	**R_0 (Ω)**	**ionic conductivity σ (mS/cm)**
PE	1.96	19	2.922	0.332
AM-CTF-PE	1.96	20.5	2.238	0.467
HC-CTF-PE	1.96	20.5	1.573	0.665

Supplementary Table 3. Specific values for t_{Li^+} calculation

	ΔV (V)	**I_0 (A)**	**I_s (A)**	**R_{el}^0(A)**	**R_{el}^s(A)**	**t_{Li^+}**
PE	0.01	$5.42*10^{-5}$	$4.90*10^{-5}$	177.74	182.32	0.31
AM-CTF-PE	0.01	$6.20*10^{-5}$	$5.70*10^{-5}$	153.43	156.32	0.41
HC-CTF-PE	0.01	$7.99*10^{-5}$	$7.46*10^{-5}$	114.4	116.19	0.60

Supplementary Table 4. Comparison of electrochemical properties of separators and assembled cells with literature.

Materials	t_{Li^+}	ionic conductivity (mS cm^{-1})	Li plating performance	Ref.
AM-CTF-PE	0.41	0.46	170 h@1 mA cm^{-2}/1 mAh cm^{-2} 80 h@1 mA cm^{-2}/1 mAh cm^{-2}	Our work
HC-CTF-PE	0.60	0.66	300 h@1 mA cm^{-2}/1 mAh cm^{-2} 100 h@2 mA cm^{-2}/2 mAh cm^{-2}	
ZIF-67-C_{60}	0.79	3.58	600 h @0.5 mA cm^{-2}/0.5 mAh cm^{-2}	[1]
PAN/amide-group-bonded COF	0.79	3.33	300 h@1 mA cm^{-2} /1 mAh cm^{-2}	[2]
TpPa-2SO_3H COF/CNF/PP	0.65	0.24	800 h@1 mA cm^{-2} /0.5 mAh cm $^{-2}$	[3]
CNFs/PE/CNFs	-	0.22	155 h@0.65 mA cm^{-2} /0.65 mAh cm^{-2}	[4]
NH_2-MIL-125	0.68	0.26	>150 h@1 mA cm^{-2}/0.5 mAh cm^{-2}	[5]
Amorphous Silica Nanosheets	0.54	1.14	2000 h@0.1 mA cm^{-2}	[6]
PPTA/LLZTO	0.57	0.323	500 h@0.5 mA cm^{-2}/1 mAh cm^{-2}	[7]
PAN/LITFSI/$Li_{6.3}La_3Zr_{1.65}W_{0.35}O_{12}$	0.58	0.069	>350 h@0.2 mA cm^{-2}/0.1 mAh cm^{-2}	[8]
$Li_{0.375}Sr_{0.375}Ta_{0.75}Zr_{0.25}O_3$@polydopamine	-	0.754	180 h@1 mA cm^{-2}	[9]

REFERENCES

1. Liang X, Zhao D, Wang L, et al. C_{60} and ZIF-67 synergistically modified gelatin-based nanofibrous separators for Li-S batteries. *Energy Mater*. 2023;3:300006. [10.20517/energymater.2022.63]
2. Wang K, Duan J, Chen X, et al. Nanofibrous covalent organic frameworks based hierarchical porous separators for fast-charging and thermally stable lithium metal batteries. *Adv Energy Mater*. 2024;13:2401146. [DOI:10.1002/aenm.202401146]
3. Wang C, Li W, Jin Y, Liu J, Wang H, Zhang Q. Functional separator enabled by covalent organic frameworks for high-performance Li metal batteries. *Small*. 2023;28:2300023. [DOI:10.1002/smll.202300023]
4. Pan R, Xu X, Sun R, et al. Nanocellulose modified polyethylene separators for lithium metal batteries. *Small*. 2018;21:1704371. [DOI:10.1002/smll.201704371]
5. Hao Z, Wu Y, Zhao Q, et al. Functional separators regulating ion transport enabled by metal-organic frameworks for dendrite-free lithium metal anodes. *Adv Funct Mater*. 2021;33:2102938. [DOI:10.1002/adfm.202102938]
6. Guo C, Luo Z, Zhou M, et al. Clay-originated two-dimensional holey silica separator for dendrite-

free lithium metal anode. *Small*. 2023;36:2301428. [DOI:10.1002/smll.202301428]

7. Mao Y, Sun W, Qiao Y, et al. A high strength hybrid separator with fast ionic conductor for dendrite-free lithium metal batteries. *Chem Eng J*. 2021;416:129119. [DOI:10.1016/j.cej.2021.129119]
8. Fu X, Shang C, Yang M, Akinoglu EM, Wang X, Zhou G. An ion-conductive separator for high safety Li metal batteries. *J Power Sources*. 2020;475:228687. [DOI:10.1016/j.jpowsour.2020.228687]
9. Huang B, Luo J, Xu B, et al. Surface coating on a separator with a reductive solid Li-ion conductor for dendrite-free Li-metal batteries. *ACS Appl Energy Mater*. 2021;8:8621-8628. [DOI:10.1021/acsaem.1c01852]